New Characterization of an Improved Numerical Method for Solving the Electrical Impedance Equation in the Plane: An Approach from the Modern Pseudoanalytic Function Theory

C. M. A. Robles G. *IAENG, Member*, A. Bucio R. *IAENG, Member* and M. P. Ramirez T. *IAENG, Member*.

***Abstract*—Employing an improved numerical method, we approach solutions for the Dirichlet boundary value forward problem of the Electrical Impedance Equation in the plane. Some of the considered conductivity functions posses an exact mathematical representation. The rest arise from geometrical figures. Both classes of conductivity functions are analyzed within bounded domains, emphasizing the results corresponding to non-smooth boundaries, for which not any additional regularization method was required.**

***Index Terms*—Bers, Impedance, Non-smooth, Pseudoanalytic, Vekua.**

I. INTRODUCTION

THE elements of the modern Pseudoanalytic Function Theory have allowed to establish the relation between the two-dimensional Electrical Impedance Equation (1), and a special class of Vekua equation [12].

More precisely, we are able to write the general solution of the equation:

$$\mathrm{div}\left(\sigma \mathrm{grad} u\right) = 0, \tag{1}$$

where σ is the conductivity function, and u denotes the electric potential, in terms of the so-called Taylor series in formal powers [2]. The relation was first noticed in [8] and [1], independently. After that, a variety of works dedicated to the exact and numerical mathematical analysis, appeared in the literature (see e.g. [7], [9] and [10]).

This new approach is very important because solving the forward problem is fundamental if we are to understand the inverse problem, commonly known as Electrical Impedance Tomography [13].

These pages are dedicated to analyze the numerical solutions for the Dirichlet boundary value forward problem of (1) in the plane, employing an improved numerical method presented in [10], and based upon a conjecture proposed in [9].

The work includes a wide variety of examples, both analytic and geometrical, for representing electrical conductivity functions. Indeed, every example is illustrated taking into account a long enough quantity of parameters, thus we can assert that we proposed a more detailed characterization of the improved numerical method, than those published previously in [10] and [11].

The experimental results reported in further pages, can be classified from two different points of view. The first perspective would separate the results in two classes: Those that correspond to exact mathematical representations of conductivity functions, and those whose conductivity functions arise from geometrical distributions. A second point of view is to classify the results according to the domain within their conductivity functions were defined. Hence, we would have those that correspond to smooth-bounded domains, and those upcoming from non-smooth-bounded domains.

The second point of view is the one to be considered, because the last example exposed in these pages, corresponds to one special case of non-smooth-bounded domain for which not any additional regularization is required for approaching the solution of the boundary value problem.

Indeed, this last example is based into a purely geometrical conductivity function, which also includes non-smooth points. Our objective is to show that even for this special class of conductivity functions, and domains, the improved numerical method is useful for approaching solutions of (1).

In this sense, the contribution of the present work is the procedure for emphasizing the property cited in the last paragraph, which was the headmost topic of [11] but where the number of base functions for approaching the boundary condition was limited, due to the technique employed for obtaining the coefficients applied in the approximation. Here we approach the boundary condition taking into account almost twice the quantity of base functions considered in [11]. Hence the current characterization shall be more representative, because the significant increment in the number of base functions enhances in the limiting cases where the method works efficiently.

The conclusions are omitted because of the large quantity of experimental results included in the work. As a matter of fact, a proper description of the behavior of the method along every posed example, is not available yet, and it would be out of the scope of this paper.

II. PRELIMINARIES

In agreement with the Pseudoanalytic Function Theory posed by L. Bers [2], we will consider a pair of complex-valued functions (F, G), that satisfy the following condition:

$$\mathrm{Im}\left(\overline{F}G\right) > 0. \tag{2}$$

C. M. A. Robles G. is with the National Polytechnique Institute, ESIME C. Mexico, cesar.robles@lasallistas.org.mx

A. Bucio R. is with the National Polytechnique Institute, UPIITA, Mexico, ari.bucio@gmail.com

M. P. Ramirez T. is with the Communications and Digital Signal Processing Group, Engineering Faculty of La Salle University, Mexico, marco.ramirez@lasallistas.org.mx.

Each author equally contributed to the research work.

(Advance online publication: 9 February 2013)

Here $\overline{F} = \mathrm{Re}F - i\mathrm{Im}F$ is the complex conjugation of F, and i is the standard imaginary unit: $i^2 = -1$.

Thus, any complex function W can be expressed by the linear combination of F and G:

$$W = \phi F + \psi G,$$

where ϕ and ψ are real-valued functions. Because of that, the pair (F, G) is called (F, G)-*generating pair*

Professor Bers also introduced the concept of the (F, G)-*derivative* of a complex function W, and the condition for its existence. The derivative is given in conformity with the expression

$$\partial_{(F,G)} W = (\partial_z \phi) F + (\partial_z \psi) G, \tag{3}$$

and only exist iff

$$(\partial_{\overline{z}} \phi) F + (\partial_{\overline{z}} \psi) G = 0, \tag{4}$$

where

$$\partial_z = \partial_x - i\partial_y, \ \ \partial_{\overline{z}} = \partial_x + i\partial_y.$$

The operators ∂_z and $\partial_{\overline{z}}$ are classically introduced with the factor $\frac{1}{2}$, but for this work it will be more convenient to work without it.

Set forth the functions

$$\begin{aligned} A_{(F,G)} &= \frac{\overline{F}\partial_z G - \overline{G}\partial_z F}{F\overline{G} - G\overline{F}}, \\ a_{(F,G)} &= -\frac{\overline{F}\partial_{\overline{z}} G - \overline{G}\partial_{\overline{z}} F}{F\overline{G} - G\overline{F}}, \\ B_{(F,G)} &= \frac{F\partial_z G - G\partial_z F}{F\overline{G} - G\overline{F}}, \\ b_{(F,G)} &= -\frac{G\partial_{\overline{z}} F - F\partial_{\overline{z}} G}{F\overline{G} - G\overline{F}}; \end{aligned} \tag{5}$$

the (F, G)-derivative expression in (3) will become

$$\partial_{(F,G)} W = \partial_z W - A_{(F,G)} W - B_{(F,G)} \overline{W}, \tag{6}$$

and the condition (4) will be written as

$$\partial_{\overline{z}} W - a_{(F,G)} W - b_{(F,G)} \overline{W} = 0. \tag{7}$$

The expressions (5) are called *characteristic coefficients* of the generating pair (F, G), whereas (7) is known as the Vekua equation [12]. Indeed, every function W solution of (7) is called an (F, G)-*pseudoanalytic* function.

The following statements were first proposed by [2], and we shall appoint that they have been adapted for the present work.

***Theorem** 1:* Every element of the (F, G)-generating pair is (F, G)-pseudoanalytic. Beside, the (F, G)-derivative of these functions, introduced in (6), vanishes:

$$\partial_{(F,G)} F = \partial_{(F,G)} G = 0.$$

***Remark** 1:* Let us consider a non-vanishing function p within a bounded domain $\Omega(\mathbb{R}^2)$. The functions

$$F_0 = p, \ \ G_0 = \frac{i}{p}, \tag{8}$$

constitute a generating pair, whose characteristic coefficients (5) are

$$\begin{aligned} A_{(F_0,G_0)} &= a_{(F_0,G_0)} = 0, \\ B_{(F_0,G_0)} &= \frac{\partial_z p}{p}, \\ b_{(F_0,G_0)} &= \frac{\partial_{\overline{z}} p}{p}. \end{aligned} \tag{9}$$

***Definition** 1:* Supposed (F_0, G_0) and (F_1, G_1) as two generating pairs in form of (9), their characteristic coefficients fulfil

$$B_{(F_1,G_1)} = -b_{(F_0,G_0)}. \tag{10}$$

Therefore, (F_1, G_1) will be referred as successor pair of (F_0, G_0), since (F_0, G_0) will be called a predecessor of (F_1, G_1).

***Definition** 2:* Considering

$$\{(F_m, G_m)\}, \ m = 0, \pm 1, \pm 2, ...$$

as a set of generating pairs, where (F_{m+1}, G_{m+1}) is always a successor of (F_m, G_m). The set $\{(F_m, G_m)\}$ will be known as a generating sequence. In addition, if there exist a number c such that $(F_m, G_m) = (F_{m+c}, G_{m+c})$ the generating sequence posses period c. Furthermore, if $(F, G) = (F_0, G_0)$, we will assert that (F, G) is embedded into $\{(F_m, G_m)\}$.

***Theorem** 2:* Let (F_0, G_0) be a generating pair of the form (8), and let p be a separable-variables function within a bounded domain $\Omega(\mathbb{R}^2)$:

$$p = p_1(x) \cdot p_2(y),$$

where $x, y \in \mathbb{R}$. Thereby, (F_0, G_0) will be embedded into a periodic generating sequence, with period $c = 2$. More precisely, for an even number m the generating pair will posses the form

$$F_m = \frac{p_2(y)}{p_1(x)}, \ G_m = i\frac{p_1(x)}{p_2(y)};$$

whereas for an odd m we have

$$F_m = p_1(x) \cdot p_2(y), \ G_m = \frac{i}{p_1(x) \cdot p_2(y)};$$

Moreover, if $p_1(x) \equiv 1, \ x \in \Omega\left(\mathbb{R}^2\right)$, it is easy to see that the generating sequence in which (F_0, G_0) is embedded, will be periodic with period $c = 1$.

L. Bers first stated the concept of the (F_0, G_0)-*integral* of a complex-valued function W. On behalf of conciseness, we refer the reader to the specialized literature [2] and [7], for a complete and detailed description of the conditions for the existence of such integral. In the following pages, every complex function contained into an (F_m, G_m)-integral will be, by definition, integrable.

***Definition** 3:* Let (F_m, G_m) be a generating pair of the form (8). According to the formulas

$$F_m^* = -iF_m, \ \ G_m^* = -iG_m;$$

are defined the elements of the *adjoin* generating pair (F_0^*, G_0^*).

***Definition** 4:* The (F_m, G_m)-integral of a complex-valued function W (if it exists [2]) is defined as:

$$\int_\tau W d_{(F_m,G_m)} z =$$

$$= F_m \mathrm{Re} \int_\tau G_m^* W dz + G_m \mathrm{Re} \int_\tau F_m^* W dz,$$

where τ is a rectifiable curve, connecting the fixed point z_0 with $z = x + iy$, within a bounded domain Ω, in the complex plane. More precisely, when considering the (F_m, G_m)-integral of the (F_m, G_m)-derivative of W, we will obtain:

$$\int_{z_0}^{z} \partial_{(F_m,G_m)} W(z) d_{(F_m,G_m)} z =$$
$$= -\phi(z_0) F_m(z) - \psi(z_0) G_m(z) + W(z). \qquad (11)$$

In agreement with the Theorem 1, the (F_m, G_m)-derivatives of F_m and G_m vanish identically. Hence the expression (11) can be taken into as the (F_m, G_m)-*antiderivative* of $\partial_{(F_m,G_m)} W$.

A. Formal Powers

Definition 5: The formal power $Z_m^{(0)}(a_0, z_0; z)$, associated to the generating pair (F_m, G_m), with formal degree 0, complex constant coefficient a_0, center at z_0, and depending upon $z = x+iy$, is defined in agreement with the expression:

$$Z_m^{(0)}(a_0, z_0; z) = \lambda F_m(z) + \mu G_m(z), \qquad (12)$$

where λ and μ are complex constants that fulfill the following condition:

$$\lambda F_m(z_0) + \mu G_m(z_0) = a_0.$$

For approaching the formal powers with higher degrees (n), it is necessary to employ the following recursive formulas:

$$Z_m^{(n)}(a_n, z_0; z) =$$
$$= n \int_{z_0}^{z} Z_{(m-1)}^{(n-1)}(a_n, z_0; z)\, d_{(F_m,G_m)} z,$$

where $n = 1, 2, 3, ...$ Notice that the integral operators in the right-hand side of the last expression are (F_m, G_m)-antiderivatives.

Theorem 3: The formal powers hold on the following properties:

1) Every $Z_m^{(n)}(a_n, z_0; z)$, being $n = 0, 1, 2, 3, ...$ is an (F_m, G_m)-pseudoanalytic function.
2) Let $a_n = a_n' + i a_n''$, where $a_n', a_n'' \in \mathbb{R}$. The following relation holds:

$$Z_m^{(n)}(a_n, z_0; z) =$$
$$= a_n' Z_m^{(n)}(1, z_0; z) + a_n'' Z_m^{(n)}(i, z_0; z). \qquad (13)$$

3) For $n = 0, 1, 2, 3, ...$ it holds that

$$\lim_{z \to z_0} Z_m^{(n)}(a_n, z_0; z) = a_n (z - z_0)^n. \qquad (14)$$

Theorem 4: Let W be an (F_m, G_m)-pseudoanalytic function. Thus, we can express it in terms of the so-called *Taylor series in formal powers*:

$$W = \sum_{n=0}^{\infty} Z_m^{(n)}(a_n, z_0; z). \qquad (15)$$

Since every (F_m, G_m)-pseudoanalytic function W accepts this expansion, (15) is an analytic representation of the general solution for the Vekua equation (9).

B. The two-dimensional Electrical Impedance Equation.

Let us consider the Electrical Impedance Equation (1) in the plane, and let the conductivity σ be a separable-variables function:

$$\sigma(x, y) = \sigma_1(x) \sigma_2(y), \qquad (16)$$

As it has been shown in several previous works (e.g. [1], [8] and [9]), introducing the following notations,

$$W = \sqrt{\sigma}\,(\partial_x u - i \partial_y u), \quad p = \left(\sigma_1^{-1} \cdot \sigma_2\right)^{\frac{1}{2}}; \qquad (17)$$

the two-dimensional case of the equation (1), can be rewritten into a Vekua equation with form

$$\partial_{\bar{z}} W - \frac{\partial_{\bar{z}} p}{p} \overline{W} = 0. \qquad (18)$$

As a matter of fact, a generating pair corresponding to this Vekua equation is

$$F_1 = p,\ G_1 = \frac{i}{p}. \qquad (19)$$

Taking into account the theorem 2, the reader can notice that this generating pair is embedded into a periodic generating sequence, with period $c = 2$, for p is separable-variables function.

C. Numerical approach of the formal powers.

In [10], it was studied an improved numerical method for approaching the elements the finite subset of formal powers:

$$\left\{ Z_0^{(n)}(1, 0; z), Z_1^{(n)}(i, 0; z) \right\}_{n=0}^{N}, \qquad (20)$$

whose linear combination will allows to approach any pseudoanalytc function W, solution of (18). Furthermore, in [5], it was proven that the real parts of the elements of (20), valued at the boundary Γ of the domain Ω, constitute a complete set to approach solutions for the Dirichlet boundary value forward problem of (1) in the plane.

Since the results of the integral expressions (11) are path-independent [2], the numerical calculations can be performed on a set of radial trajectories, whose origin coincides with the zero of the plane. Thus, the following procedure will be employed in each radius R within the domain Ω, going from the coordinates origin until the boundary Γ.

Let us consider τ as a radius R within, *e.g.*, the unitary circle with center at $z_0 = 0$. For the interpolation process, we will use $P + 1$ points equidistantly distributed on R, being the first $r[0] = 0$ and the last $r[P] = 1$:

$$\left\{ r[p] = \frac{p}{P} \right\}_{p=0}^{P}. \qquad (21)$$

We can immediately construct a set of coordinates according to the formulas:

$$x[p] = r[p] \cos\theta_q, \quad y[p] = r[p] \sin\theta_q; \qquad (22)$$

where θ_q is the angle that matches to R. In agreement with (8), the coordinates (22) will be employed to obtain the sets of values

$$\{F_0(z[p]), G_0(z[p])\},\ \{F_1(z[p]), G_1(z[p])\}; \qquad (23)$$

where the complex numbers $z[p]$ have the form:

$$z[p] = x[p] + iy[p].$$

The set of values of the adjoin pairs

$$\{F_0^*(z[p]), G_0^*(z[p])\},\ \{F_1^*(z[p]), G_1^*(z[p])\} \tag{24}$$

will have the form shown in the Definition 3.

From the expression (5), it follows that

$$\begin{aligned} Z_0^{(0)}(1,0;z[p]) &= F_0(z[p]), \\ Z_1^{(0)}(1,0;z[p]) &= F_1(z[p]); \end{aligned}$$

Hereafter, each formal power with $n > 0$ will be always approached considering $P+1$ equidistant points within the closed interval $[0,1]$. Taking into account that not any methodological difference takes place when approaching the formal power with coefficients $a_n = i$, we will focus our explanation for the cases when $a_n = 1$.

At this point, a numerical property first noticed in [9], for approaching the formal powers, can significantly reduce the computational resources invested in the complete procedure, at the time it allows to employ the posed method for analyzing non-separable variables conductivity functions.

The following statements were presented and proved in [9], together with some representative examples.

***Conjecture** 1:* Let σ be an arbitrary conductivity function defined within a bounded domain $\Omega\left(\mathbb{R}^2\right)$. It can be approached by means of a piece-wise separable-variables function of the form:

$$\sigma_{pw} = \begin{cases} \frac{x+g}{\chi_1-\chi_0+g}\cdot f_1(y) & : \quad x \in [\chi_0,\chi_1)\,; \\ \frac{x+g}{\chi_2-\chi_1+g}\cdot f_2(y) & : \quad x \in [\chi_1,\chi_2)\,; \\ \vdots & \\ \frac{x+g}{\chi_K-\chi_{K-1}+g}\cdot f_K(y) & : \quad x \in [\chi_{K-1},\chi_K]\,; \end{cases}$$

where g is a real constant such that $x+g \neq 0 : x \in \Omega\left(\mathbb{R}^2\right)$; and $\{f_k\}_{k=1}^K$ are interpolating functions constructed with a finite number of samples $\mathcal{M}$ of the function σ, valued along an y-axis parallel line within the subdomains of Ω, created when tracing the set of y-axis parallel lines $\{\chi_k\}_{k=0}^K$. This piece-wise separable-variables conductivity function can be employed for numerically approaching the set of formal powers (24).

***Proposition** 1:* [9] Let σ be an arbitrary conductivity function defined within a bounded domain $\Omega\left(\mathbb{R}^2\right)$. It can be considered as the limiting case of a piece-wise separable-variables function, with the form presented in the Conjecture 1, when the number of subdomains K and the number of samples $\mathcal{M}$ at every subdomain, tend to infinite:

$$\lim_{K,\mathcal{M}\to\infty} \sigma_{pw} = \sigma.$$

Furthermore, since:

$$\lim_{K,\mathcal{M}\to\infty} \frac{x+g}{\chi_k-\chi_{k-1}+g} = 1,\ k = 0,1,...,K;$$

according to the Theorem 2, the corresponding generating sequence will be periodic with period $c = 1$. This immediately implies that

$$F_0(z[p]) = F_1(z[p]) = F(z[p]),$$

that shall simplify the construction of the sets (23) and (24).

Employing this property, the numerical formal powers $Z_0^{(n)}(z[p])$ at the points $z[p] = x[p] + iy[p]$, located along the radius R, can be approached employing a variation of the trapezoidal integration method over the complex plane:

$$\begin{gathered} Z^{(n)}(z[p]) = \delta F(z[p]) \cdot \\ \cdot \mathrm{Re} \sum_{s=0}^{p-1} \left(Z^{(n-1)}(z[s+1]) \cdot G^*\left(z[s+1]\right)\right) dz[s] + \\ + \delta F(z[p]) \mathrm{Re} \sum_{s=0}^{p} \left(Z_1^{(n-1)}(z[s]) \cdot G^*\left(z[s]\right)\right) dz[s] + \\ + \delta G(z[p]) \cdot \\ \cdot \mathrm{Re} \sum_{s=0}^{p-1} \left(Z_1^{(n-1)}(z[s+1]) \cdot F^*\left(z[s+1]\right)\right) dz[s] + \\ + \delta G(z[p]) \mathrm{Re} \sum_{s=0}^{p} \left(Z_1^{(n-1)}(z[s]) \cdot F^*\left(z[s]\right)\right) dz[s]; \end{gathered} \tag{25}$$

where

$$dz[s] = \left(z[s+1] - z[s]\right),$$

and δ is a real constant factor, empirically selected, that contributes to the numerical stability of the method.

We shall remark that the use of the expression (25), for approaching the formal powers, as it was appointed in [9], implicitly performs a piecewise interpolating polynomial function of degree 1, to relate every value $Z^{(n)}(z[p])$, for $p = 0,1,...,P$; and $n = 0,1,...,N$; taking into consideration the third property of the Theorem 3, that implies $\forall n > 0$:

$$Z_0^{(n)}(1,0;z[0]) \equiv 0.$$

Performing the full procedure for a wide enough quantity Q of radii R, each one corresponding to some angle θ_q:

$$\left\{\theta_q = q \cdot \frac{2\pi}{Q}\right\}_{q=0}^{Q-1}, \tag{26}$$

we will be able to approach the finite set

$$\left\{\mathrm{Re} Z^{(n)}\left(1,0;z\right),\ \mathrm{Re} Z^{(n)}\left(i,0;z\right)\right\}_{n=0}^{N}, \tag{27}$$

that once is valued at the boundary Γ of the domain $\Omega\left(\mathbb{R}^2\right)$, will provide a set of $2N+1$ base functions for approaching solutions of the Dirichlet boundary value forward problem of (1), when a boundary condition $u_{\mathbf{c}}|_\Gamma$ is imposed.

Indeed, the set (27) can be orthonormalized, conforming a new base

$$\{\upsilon_0^{(n)}(l)\}_{n=0}^{2N},\ l \in \Gamma, \tag{28}$$

that can be interpolated by standard methods in order to obtain continuous functions at Γ.

Summarizing, if the number of radii R, points per radius P, and base functions $2N+1$, are adequate (as it will be explained further), a boundary condition $u_{\mathbf{c}}|_\Gamma$ can be approached by the linear combination:

$$u_{\mathbf{c}}|_\Gamma \sim \sum_{k=0}^{2N+1} \beta_k \upsilon_k,$$

where the real constant coefficients β_k are approached by the standard inner product

$$\beta_k = \langle \upsilon_k, u_{\mathbf{c}}|_\Gamma \rangle = \int_\Gamma \upsilon_k(l) \cdot u_{\mathbf{c}}|_\Gamma(l) dl. \tag{29}$$

III. Experimental Results.

We will perform a characterization of the method, using two classes of domains, and a variety of conductivity functions. This characterization employs the optimized method, first exposed in [10], using the Pseudoanalytic Function Theory, and taking into account that we can analyze any conductivity function, approaching the solution for the Dirichlet boundary value forward problem.

In this work, we will empathize the behavior of the method employing it into non-smooth domains, and comparing its effectiveness with the results obtained when analyzing the unitary disk. For both cases, we will use conductivity functions with exact representation. More precisely, we will examine exponential, Lorentzian, sinusoidal and polynomial functions. But we will also study conductivity functions upcoming from geometrical distributions, such like concentric circles, a circle out of center but within the domain, and a square.

A. The Unit Circle Domain.

The behavior of the method for this case, whenever the conductivity possesses a separable-variables form or not, is particularly stable. We refer the reader to the previous works [3] and [10] for more details.

Here we will propose a methodology that reaches the best approximation of the method, employing the Lebesgue measure for introducing an error parameter $\mathcal{E}$:

$$\mathcal{E} = \left(\int_{\Gamma} \left(u_{\mathbf{c}}|_{\Gamma} - u_{app} \right)^2 dl \right)^{\frac{1}{2}}. \tag{30}$$

where u_{app} represents the approached solution, according to (21).

Employing a variation of the algorithm posed in [10], we will only modify the number of formal powers N, since according to the work cited before, we know that employing a bigger number of formal powers riches, a better convergence. Also, we have detected that the number of radii R, and of points per radius P, do not introduce significant variations of $\mathcal{E}$. That is why we will fix $R = P = 200$.

1) An Exponential Conductivity Case: We will consider a non-separable variables exponential conductivity function with the form

$$\sigma = e^{\alpha xy}, \tag{31}$$

where α represents a coefficient that is used to change the behavior of the function. In this case we impose the boundary condition:

$$u|_{\Gamma} = e^{-\alpha xy}. \tag{32}$$

because it is an exact solution of (1), as appointed in [9]. Hereafter, we will employ the notation

$$M = 2N + 1.$$

We shall remember that Q represents the number of radii.

The Table I shows that when the maximum number of formal powers increases, the convergence improves.

TABLE I
Exponential conductivity function $\sigma = e^{-\alpha xy}$.

M	P	Q	α	$\mathcal{E}$
121	200	200	2	6.8875×10^{-15}
81	200	200	2	7.3145×10^{-15}
41	200	200	2	1.1101×10^{-6}
121	200	200	6	3.4109×10^{-14}
81	200	200	6	3.4243×10^{-14}
41	200	200	6	1.1768×10^{-7}
121	200	200	10	4.2244×10^{-14}
81	200	200	10	4.3088×10^{-14}
41	200	200	10	2.3561×10^{-6}

2) Lorentzian Conductivity Function: For this case we propose a conductivity function with the form:

$$\sigma = \left((x + d_x)^2 + L_c \right)^{-1} \cdot \left((y + d_y)^2 + L_c \right)^{-1}, \tag{33}$$

where d_x and d_y represent displacements over the x-axis and y-axis respectively, and L_c denotes a real constant.

We will imposed the boundary condition [9]:

$$u|_{\Gamma} = \frac{1}{3}(x+d_x)^3 + \frac{1}{3}(y+d_y)^3 + L_c(x+d_x+y+d_y); \tag{34}$$

since it is an exact solution of (1).

TABLE II
Lorentzian conductivity function.

M	P	Q	L_c	$\mathcal{E}$
121	200	200	0.2	2.4113×10^{-13}
81	200	200	0.2	2.1746×10^{-9}
41	200	200	0.2	2.5924×10^{-5}
121	200	200	0.4	1.5266×10^{-15}
81	200	200	0.4	3.8584×10^{-12}
41	200	200	0.4	1.2505×10^{-6}
121	200	200	0.6	2.1483×10^{-15}
81	200	200	0.6	4.3463×10^{-14}
41	200	200	0.6	1.4775×10^{-7}
121	200	200	0.8	2.1948×10^{-15}
81	200	200	0.8	2.5350×10^{-15}
41	200	200	0.8	2.7502×10^{-8}

We propose $L_c = \{0.2, 0.4, 0.6, 0.8\}$, whereas, for this case, $d_x = d_y = 0$. In the Table II the reader can notice that, every time the number of formal powers increases, the error decreases considerably. We also notice that if we use a small value of L_c, the error grows significantly.

3) Polynomial Conductivity Function: In this case, we use a polynomial conductivity function:

$$\sigma = \alpha + Cx + Cy, \tag{35}$$

imposing a boundary condition

$$u|_{\Gamma} = \ln(\alpha + Cx + Cy), \tag{36}$$

where α and C are constants such that $\alpha + Cx + Cy > 0, \ \forall x, y \in \Omega$ [9].

The Table III, shows that the increment of M provides better convergence.

4) Sinusoidal Conductivity Function: Let us consider a conductivity function with the form

$$\sigma = (\alpha + \cos\omega\pi x)(\alpha + \sin\omega\pi y), \tag{37}$$

We selected to impose a boundary condition:

$$u|_{\Gamma} = \left(\frac{\tan xy}{2} + 1 \right)^{-1}. \tag{38}$$

TABLE III
POLYNOMIAL CONDUCTIVITY FUNCTION $\sigma = \alpha + Cx + Cy$.

M	P	Q	α	C	$\mathcal{E}$
121	200	200	10	2	5.4318×10^{-15}
81	200	200	10	2	5.4318×10^{-15}
41	200	200	10	2	5.4398×10^{-15}
121	200	200	10	4	4.2384×10^{-15}
81	200	200	10	4	4.2384×10^{-15}
41	200	200	10	4	5.2431×10^{-12}
121	200	200	10	6	5.5207×10^{-15}
81	200	200	10	6	5.9757×10^{-12}
41	200	200	10	6	1.3718×10^{-6}

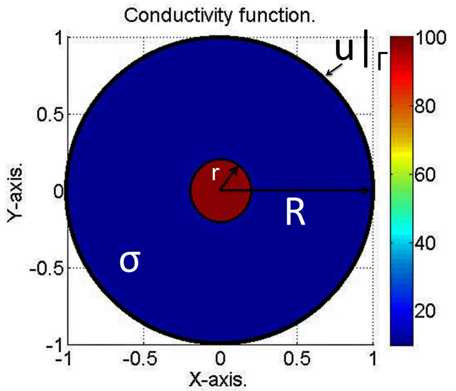

Fig. 1. First Geometrical Case: Two disks within the domain Ω, whose centers coincide.

It is necessary to remark that this function is not an exact solution of (1). Indeed, as posed in [9], it is an exact solution only for the case when $\sigma = 1 + \sin xy$. But the example becomes interesting when pointing out that, in general, the exact solutions of (1) when σ possesses the form (37), are unknown. Thus, this example is included to better illustrate the effectiveness of the method when arbitrary parameters are introduced in the analysis.

TABLE IV
SINUSOIDAL CONDUCTIVITY FUNCTION.

M	P	Q	α	ω	$\mathcal{E}$
121	200	200	5	2	7.8123×10^{-12}
41	200	200	5	2	8.5330×10^{-5}
121	200	200	5	6	4.5940×10^{-5}
41	200	200	5	6	2.7620×10^{-2}
121	200	200	5	10	3.5433×10^{-3}
41	200	200	5	10	1.9455×10^{-1}
121	200	200	10	2	1.2539×10^{-14}
41	200	200	10	2	9.2312×10^{-6}
121	200	200	10	6	4.0830×10^{-6}
41	200	200	10	6	1.1964×10^{-2}
121	200	200	10	10	8.5638×10^{-4}
41	200	200	10	10	9.7005×10^{-2}

The Table IV shows that when we increase M, we obtain a better convergence, but the results are the opposite if α or ω increase. In this sense, the Table IV offers the opportunity for establishing a limiting example for which the method is valid.

5) First Geometrical Case: We propose a geometrical conductivity distribution inside the domain Ω, displayed in the Figure 1. It consists of two disks, whose centers coincide at the origin. The red section represents $\sigma = 100$, whereas the blue section indicates $\sigma = 10$. The radius of the red

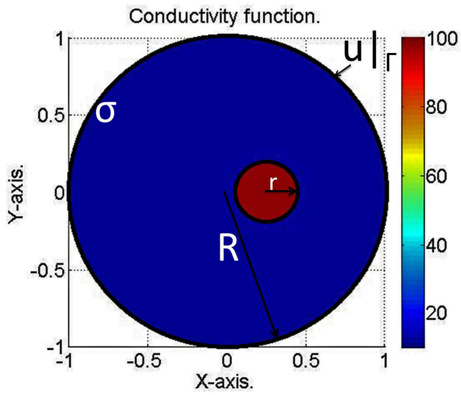

Fig. 2. Disk displaced from the center. Any other displacement can be considered a rotation of this example.

section is denoted by r.

As it was previously indicated in [9], to establish a boundary condition without performing physical measurements, becomes a non-trivial task for conductivity functions arising from geometrical figures. That is why, hereafter, we will employ the boundary condition (34). The selection of this condition was arbitrary, being useful only for appreciating the behavior of the numerical method.

TABLE V
FIRST GEOMETRICAL CASE: RD INDICATES THE VALUE OF THE RED DISK, WHEREAS BD REPRESENTS THE BLUE DISK.

M	P	Q	r	RD	BD	$\mathcal{E}$
121	200	200	0.2	10	100	5.3266×10^{-15}
41	200	200	0.2	10	100	7.1940×10^{-15}
121	200	200	0.4	10	100	6.0657×10^{-15}
41	200	200	0.4	10	100	8.1351×10^{-15}
121	200	200	0.6	10	100	4.3213×10^{-15}
41	200	200	0.6	10	100	5.2102×10^{-15}
121	200	200	0.8	10	100	3.4712×10^{-15}
41	200	200	0.8	10	100	4.4355×10^{-15}

The Table V shows that the convergence increments when the number of formal powers M slightly increase. This behavior is also present when changing the magnitude of the radius r, exception done for the case when $r \sim \mathbf{R}$, the radius of the unit circle.

6) A variation of the First Geometrical Case: The alteration is the displacement of the disk with conductivity $\sigma = 100$, whose center is located at $x = 0.25,\ y = 0$.

Once more, the boundary condition is a variation of (34), noticing that, on behalf of simplicity, we have fixed $L_c = 0.5$, as displayed in Figure 2:

$$u|_\Gamma = \frac{1}{3}(x + 0.25)^3 + \frac{1}{3}y^3 + 0.5(x + 0.25 + y),$$

The table VI illustrates that if we use a bigger number of base functions M, the convergence increases, but what it becomes interesting with this example is the diameter of the red disk, which provokes significant variations in the convergence. Notice any other displacement of the interior disk, can be considered a geometrical rotation to the case we have studied in this section. Thus, the numerical results are fully equivalent to those reported here.

7) Second Geometrical Case: We propose a geometrical conductivity function consisting in one disk and four rings,

TABLE VI
VARIATION OF THE FIRST GEOMETRICAL CASE: RD INDICATES THE VALUE OF THE RED DISK, WHEREAS BD REPRESENTS THE BLUE DISK.

M	P	Q	r	RD	BD	$\mathcal{E}$
121	200	200	0.2	10	100	3.8194×10^{-2}
41	200	200	0.2	10	100	8.4548×10^{-2}
121	200	200	0.4	10	100	4.6197×10^{-3}
41	200	200	0.4	10	100	7.2787×10^{-3}
121	200	200	0.6	10	100	3.2798×10^{-3}
41	200	200	0.6	10	100	4.4617×10^{-3}
121	200	200	0.8	10	100	9.8760×10^{-2}
41	200	200	0.8	10	100	2.0676×10^{-1}

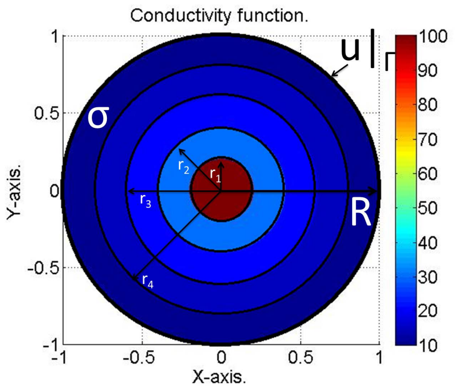

Fig. 3. Concentric disk and rings. The disk $r_1 = 0.2$ represents $\sigma = 100$; the ring delimited by the circles $r_2 = 0.4$ and r_1 represents $\sigma = 30$; for $r_3 = 0.6$ and r_2 we have $\sigma = 20$; for $r_4 = 0.8$ and r_3 it is $\sigma = 15$; finally for $\mathbf{R} = 1$ and r_4 we have $\sigma = 10$.

within the unit circle, whose centers concur, as displayed in Figure 3. The disk with radius $r_1 = 0.2$ represents $\sigma = 100$, the ring delimited by $r_2 = 0.4$ and r_1 possesses a conductivity $\sigma = 30$. For the ring between $r_3 = 0.6$ and r_2 we have $\sigma = 20$, whereas for the one within $r_4 = 0.8$ and r_3 exhibits $\sigma = 15$. Finally, the exterior ring delimited by $\mathbf{R} = 1$ and r_4 the conductivity is $\sigma = 10$.

The imposed boundary condition will be

$$u|_\Gamma = \frac{1}{3}(x^3 + y^3) + 0.5(x + y).$$

The table VII shows that when the number M increases, the convergence improves. It is interesting that the value of the error $\mathcal{E}$ does not increase by the diminution of the base functions M.

TABLE VII
A CONDUCTIVITY FUNCTION COMPOSED BY ONE DISK AND FOUR RINGS. HERE THE NUMBER OF RADII AND THE POINTS PER RADIUS ARE BOTH FIXED AT 200.

M	P	Q	$\mathcal{E}$
121	200	200	3.0440×10^{-15}
101	200	200	3.0216×10^{-15}
61	200	200	2.9303×10^{-15}
21	200	200	2.8133×10^{-15}

The Table VIII illustrates another interesting property of this example, for the error $\mathcal{E}$ does not experience significant changes when increasing the number of radii R and the number of points per radius Q. Nevertheless, the smaller error appears when less base functions are employed. This characteristic shall be studied with more detail in other works.

TABLE VIII
A CONDUCTIVITY FUNCTION COMPOSED BY ONE DISK AND FOUR RINGS. A COMPLEMENTARY EXAMPLE.

M	P	Q	$\mathcal{E}$
61	1000	200	5.0324×10^{-15}
61	600	200	5.4919×10^{-15}
61	200	200	2.9303×10^{-15}
41	1000	200	4.8146×10^{-15}
41	600	200	5.3062×10^{-15}
41	200	200	2.8885×10^{-15}
21	1000	200	4.3974×10^{-15}
21	600	200	4.9358×10^{-15}
21	200	200	2.8133×10^{-15}

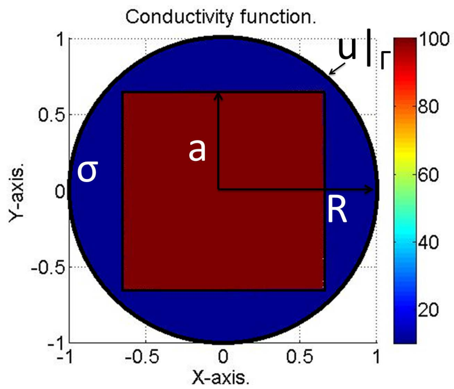

Fig. 4. A non-smooth figure is located within the unitary circle. One radius has been located at every non-smoothness of the square, being $a = 0.65$, so they are necessarily considered in the calculations.

8) Third Geometrical Case. A Non-Smooth Figure Within the Unit Circle: This case is representative because it could require additional regularization techniques, if it was solved with classical methods, as the variations of the Finite Element Method. The figure into the domain is a perfect square, whose apothem is $a = 0.65$. Beside, every corner of the square has the same distance to the center of the unit circle. We forced four radii to cross every corner, thus the non-smoothness of the figure is effectively considered into the calculations. The area of the square will represent $\sigma = 100$, whereas the rest of the domain will possess $\sigma = 10$.

The boundary condition, once more, will be:

$$u|_\Gamma = \frac{1}{3}(x^3 + y^3) + 0.5(x + y).$$

When compared to the other examples, the Table IX illustrates that the error $\mathcal{E}$ is considerably bigger. To explain this, we shall point out that the boundary condition was arbitrarily imposed, thus the error is expected to decrease when a physical measured is performed. Still, we could assert that the convergence of the method is stable from a certain point of view, since $\mathcal{E}$ decreases when the number of base functions M grows.

TABLE IX
A NON-SMOOTH FIGURE LOCATED WITHIN THE UNITARY CIRCLE.

M	P	Q	$\mathcal{E}$
121	200	200	1.3229×10^{-2}
101	200	200	1.6389×10^{-2}
81	200	200	2.2319×10^{-2}
61	200	200	3.0232×10^{-2}
41	200	200	5.4568×10^{-2}
21	200	200	1.1610×10^{-1}

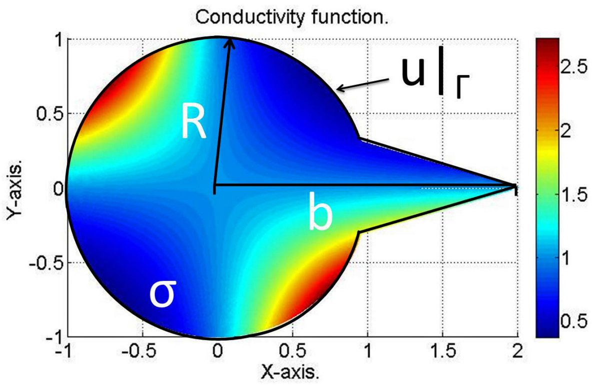

Fig. 5. Non-smooth conductivity exponential case.

We shall also enhance that, according to the information of the Table X, the convergence of the method does not improve when increasing the number of radii R and the number of points per radius Q.

TABLE X
A NON-SMOOTH FIGURE LOCATED WITHIN THE UNITARY CIRCLE: A COMPLEMENTARY EXAMPLE.

M	P	Q	$\mathcal{E}$
121	500	500	2.9031×10^{-2}
101	500	500	3.2493×10^{-2}
81	500	500	3.8417×10^{-2}
61	500	500	4.6756×10^{-2}
41	500	500	6.7906×10^{-2}
21	500	500	1.2200×10^{-1}

B. Brief Study of Conductivity Functions Within a Non-Smooth Domain.

The Figure 5 illustrate a domain Ω conformed by a unit circle with radius $\mathbf{R} = 1$, just as in the examples posed before, but only defined within the interval $x \in \left(-1, \cos\frac{\pi}{10}\right)$; and a triangular area quoted by the line segments $y_0(x) = \cos\frac{\pi}{10}$, $y_1 = \mathbf{k}_1 x + \mathbf{k}_2$ and $y_2 = -\mathbf{k}_1 x + \mathbf{k}_2$. Indeed, we will employ the same parameters posed in [9] and [11]. This is: $\mathbf{k}_1 = 0.5629$ and $\mathbf{k}_2 = 0.8443$. It will be also useful to introduce a parameter b, that will denote the distance between the coordinates origin and the intersection of the lines y_1 and y_2.

We remark that, for all cases shown further, the boundary conditions do not correspond to analytic solutions of (1), but they are all variations of a Lorentzian case. This will allow us to enhance the effectiveness of the method in what it could be considered exalted non-smoothness points at the boundary Γ.

Notice that the reference to the Figure 5 is exclusively for illustrating the shape of the non-smooth domain, since every example will consider a different class of conductivity.

1) An Exponential Conductivity Function: As before, let us suppose a conductivity function with the form

$$\sigma = e^{\alpha xy},$$

We will examine the cases $\alpha = 2, 4, 6, 8, 10$, imposing the boundary condition (34), noticing only that it will be valued, as all cases hereafter, at the boundary Γ of the domain presented in the paragraph above.

TABLE XI
EXPONENTIAL CONDUCTIVITY FUNCTION IN A NON-SMOOTH DOMAIN: $\sigma = e^{\alpha xy}$.

M	P	Q	b	α	$\mathcal{E}$
121	200	200	1.0	2	7.7189×10^{-5}
101	200	200	1.0	2	1.1321×10^{-4}
41	200	200	1.0	2	5.4926×10^{-4}
21	200	200	1.0	2	2.3060×10^{-3}
121	200	200	1.0	4	1.8890×10^{-4}
101	200	200	1.0	4	2.4912×10^{-4}
41	200	200	1.0	4	9.7697×10^{-4}
21	200	200	1.0	4	4.1727×10^{-3}
121	200	200	1.0	6	3.8650×10^{-6}
101	200	200	1.0	6	5.3340×10^{-4}
41	200	200	1.0	6	1.1522×10^{-3}
21	200	200	1.0	6	8.2815×10^{-3}
121	200	200	1.0	8	5.8860×10^{-5}
101	200	200	1.0	8	8.2280×10^{-4}
41	200	200	1.0	8	3.4367×10^{-3}
21	200	200	1.0	8	1.5269×10^{-2}
121	200	200	1.0	10	7.5198×10^{-4}
101	200	200	1.0	10	1.0642×10^{-3}
41	200	200	1.0	10	4.6709×10^{-3}
21	200	200	1.0	10	3.2356×10^{-2}

For the Table XI, we do observe a diminution of the error when increasing the number of base functions M. Notice we have fixed the parameter $b = 1$.

As a complementary experiment, the table XII shows the results of the case when we fix $b = 1.5$.

TABLE XII
EXPONENTIAL CONDUCTIVITY FUNCTION IN NON-SMOOTH DOMAIN: SECOND EXAMPLE.

M	P	Q	b	α	$\mathcal{E}$
121	200	200	1.5	2	1.9190×10^{-3}
101	200	200	1.5	2	1.4889×10^{-3}
41	200	200	1.5	2	3.8482×10^{-4}
21	200	200	1.5	2	6.1853×10^{-4}
121	200	200	1.5	4	7.8734×10^{-3}
101	200	200	1.5	4	4.6606×10^{-3}
41	200	200	1.5	4	1.5679×10^{-3}
21	200	200	1.5	4	5.5688×10^{-3}
121	200	200	1.5	6	5.5224×10^{-3}
101	200	200	1.5	6	5.0001×10^{-3}
41	200	200	1.5	6	3.0569×10^{-3}
21	200	200	1.5	6	1.2475×10^{-2}
121	200	200	1.5	8	1.1044×10^{-2}
101	200	200	1.5	8	8.9217×10^{-3}
41	200	200	1.5	8	4.5972×10^{-3}
21	200	200	1.5	8	2.2350×10^{-2}
121	200	200	1.5	10	2.0529×10^{-2}
101	200	200	1.5	10	1.2371×10^{-2}
41	200	200	1.5	10	6.1075×10^{-3}
21	200	200	1.5	10	4.1741×10^{-2}

The Table XII displays an abnormal behavior, since the error $\mathcal{E}$ does not decrease as the number of base functions M grows. The behavior becomes even more interesting when performing the experiment for $b = 2$. The table XIII shows that, for the cases when α is big enough, the error increases when M does. For this, it is convenient to remark that the non-smoothness is notorious.

We do not show the behavior when a variation is introduced in the number of radii R, since it affects only when a geometrical figure is placed within the domain. This analysis will be exposed in further paragraphs.

2) Lorentzian Conductivity Function: Let us propose σ in the form (33), imposing the condition (34).

TABLE XIII
EXPONENTIAL CONDUCTIVITY FUNCTION IN NON-SMOOTH DOMAIN: A THIRD EXAMPLE.

M	P	Q	b	α	$\mathcal{E}$
121	200	200	2.0	2	2.9221×10^{-2}
101	200	200	2.0	2	2.2211×10^{-2}
41	200	200	2.0	2	4.7667×10^{-3}
21	200	200	2.0	2	1.0047×10^{-2}
121	200	200	2.0	4	2.9221×10^{-2}
101	200	200	2.0	4	2.2211×10^{-2}
41	200	200	2.0	4	4.7667×10^{-3}
21	200	200	2.0	4	1.0047×10^{-2}
121	200	200	2.0	6	2.9221×10^{-2}
101	200	200	2.0	6	2.2211×10^{-2}
41	200	200	2.0	6	4.7607×10^{-3}
21	200	200	2.0	6	1.0047×10^{-2}
121	200	200	2.0	8	2.5025×10^{-1}
101	200	200	2.0	8	1.8884×10^{-1}
41	200	200	2.0	8	1.5368×10^{-2}
21	200	200	2.0	8	3.6063×10^{-2}
121	200	200	2.0	10	6.8271×10^{-1}
101	200	200	2.0	10	4.9283×10^{-1}
41	200	200	2.0	10	2.1281×10^{-2}
21	200	200	2.0	10	6.4350×10^{-2}

Employing the methodology posed above, we begin the experiments fixing $P = Q = 200$, considering $b = 1$. The results are shown in the table XIV. Similarly to the exponential case with $b = 1$ in the non-smooth domain, the increment of the number of base functions M gives to us a better convergence in the numerical method. And once more, this is not valid when $b = 1.5$, as showed in the Table XV. Moreover, the Table XVI indicates that for such non-smoothness, when $b = 2$, the method presents an unexpected behavior, since when M increases, the error $\mathcal{E}$ changes without a clear pattern.

TABLE XIV
LORENTZIAN CONDUCTIVITY FUNCTION IN NON-SMOOTH DOMAIN.

M	P	Q	b	L_c	$\mathcal{E}$
121	200	200	1.0	0.2	3.7046×10^{-4}
101	200	200	1.0	0.2	5.4768×10^{-4}
41	200	200	1.0	0.2	2.5055×10^{-3}
21	200	200	1.0	0.2	7.8163×10^{-3}
121	200	200	1.0	0.4	3.7511×10^{-4}
101	200	200	1.0	0.4	5.5286×10^{-4}
41	200	200	1.0	0.4	2.5378×10^{-3}
21	200	200	1.0	0.4	8.9281×10^{-3}
121	200	200	1.0	0.6	3.8343×10^{-4}
101	200	200	1.0	0.6	5.6391×10^{-4}
41	200	200	1.0	0.6	2.6002×10^{-3}
21	200	200	1.0	0.6	9.3482×10^{-3}
121	200	200	1.0	0.8	3.9114×10^{-4}
101	200	200	1.0	0.8	5.7438×10^{-4}
41	200	200	1.0	0.8	2.6563×10^{-3}
21	200	200	1.0	0.8	9.6121×10^{-3}

3) Polynomial Conductivity Function: Let us propose a conductivity function with the form (35), with a boundary condition (34). The behavior is regular when $b = 1$, as displayed in the values of the Table XVII. But once again, when $b = 1.5$, we can not notice the presence of a pattern, as the reader can verify in the Table XVIII. The method behaves abnormally when $b = 2$, according to the values of the Table XIX.

TABLE XV
LORENTZIAN CONDUCTIVITY FUNCTION IN NON-SMOOTH DOMAIN: A SECOND EXAMPLE.

M	P	Q	b	L_c	$\mathcal{E}$
121	200	200	1.5	0.2	2.1045×10^{-2}
101	200	200	1.5	0.2	1.3569×10^{-2}
41	200	200	1.5	0.2	3.9952×10^{-3}
21	200	200	1.5	0.2	1.5850×10^{-2}
121	200	200	1.5	0.4	1.4743×10^{-2}
101	200	200	1.5	0.4	9.4131×10^{-3}
41	200	200	1.5	0.4	3.6909×10^{-3}
21	200	200	1.5	0.4	1.3262×10^{-2}
121	200	200	1.5	0.6	1.9460×10^{-2}
101	200	200	1.5	0.6	1.2236×10^{-2}
41	200	200	1.5	0.6	3.5889×10^{-3}
21	200	200	1.5	0.6	1.2248×10^{-2}
121	200	200	1.5	0.8	2.5640×10^{-2}
101	200	200	1.5	0.8	1.6610×10^{-2}
41	200	200	1.5	0.8	3.5508×10^{-3}
21	200	200	1.5	0.8	1.1735×10^{-2}

TABLE XVI
LORENTZIAN CONDUCTIVITY FUNCTION IN NON-SMOOTH DOMAIN: A THIRD EXAMPLE.

M	P	Q	b	L_c	$\mathcal{E}$
121	200	200	2.0	0.2	2.7463×10^{-1}
101	200	200	2.0	0.2	2.0323×10^{-1}
41	200	200	2.0	0.2	1.9108×10^{-2}
21	200	200	2.0	0.2	4.3151×10^{-2}
121	200	200	2.0	0.4	1.9367×10^{-2}
101	200	200	2.0	0.4	1.8948×10^{-2}
41	200	200	2.0	0.4	1.5901×10^{-2}
21	200	200	2.0	0.4	3.5373×10^{-2}
121	200	200	2.0	0.6	2.8857×10^{-2}
101	200	200	2.0	0.6	2.4264×10^{-2}
41	200	200	2.0	0.6	1.4621×10^{-2}
21	200	200	2.0	0.6	3.2738×10^{-2}
121	200	200	2.0	0.8	2.1095×10^{-1}
101	200	200	2.0	0.8	1.5468×10^{-1}
41	200	200	2.0	0.8	1.3982×10^{-2}
21	200	200	2.0	0.8	3.1410×10^{-1}

4) Sinusoidal Conductivity Function: Suppose that the conductivity function is expressed as

$$\sigma = (\alpha + \cos\omega\pi x)(\alpha + \sin\omega\pi y), \tag{39}$$

where α is a coefficient such that $\sigma > 1$. For this case, the condition to be imposed is

$$u|_\Gamma = \frac{1}{3}(x^3 + y^3) + 0.5(x + y). \tag{40}$$

The Table XX reports that the behavior for $b = 1$ becomes unstable when $\omega > 4$. According to the Table XXI, when $b = 1.5$, the method becomes unstable when $\omega > 6$, which was indeed not expected when analyzing the previous examples of conductivity functions. Already in the Table XXII we observe that the error $\mathcal{E}$ behaves without a pattern for $\omega > 4$.

5) First Example of Geometrical Conductivity: Let us consider a geometrical conductivity function σ, such as the one posed in the Figure 6, a circle whose center coincides with the origin and with radius $r = 0.2$, also possessing a conductivity $\sigma = 100$, whereas the rest of the non-smooth domain has $\sigma = 10$.

For this example, the imposed condition is (40). The table XXIII indicates the existence of a pattern between the number of base functions M and the error $\mathcal{E}$, for the case $b = 1$.

TABLE XVII
POLYNOMIAL CONDUCTIVITY IN A NON-SMOOTH DOMAIN.

M	P	Q	b	α	C	$\mathcal{E}$
121	200	200	1.0	10	2	1.4507×10^{-4}
101	200	200	1.0	10	2	2.0777×10^{-4}
41	200	200	1.0	10	2	9.4643×10^{-4}
21	200	200	1.0	10	2	3.5689×10^{-3}
121	200	200	1.0	10	4	1.2662×10^{-4}
101	200	200	1.0	10	4	1.7973×10^{-4}
41	200	200	1.0	10	4	8.1138×10^{-4}
21	200	200	1.0	10	4	3.1555×10^{-3}
121	200	200	1.0	10	6	1.0788×10^{-4}
101	200	200	1.0	10	6	1.5092×10^{-4}
41	200	200	1.0	10	6	6.6334×10^{-4}
21	200	200	1.0	10	6	2.7058×10^{-3}

TABLE XVIII
POLYNOMIAL CONDUCTIVITY IN NON-SMOOTH DOMAIN: SECOND EXAMPLE.

M	P	Q	b	α	C	$\mathcal{E}$
121	200	200	1.5	10	2	5.1091×10^{-3}
101	200	200	1.5	10	2	3.3772×10^{-3}
41	200	200	1.5	10	2	1.1974×10^{-3}
21	200	200	1.5	10	2	3.2404×10^{-3}
121	200	200	1.5	10	4	3.4689×10^{-3}
101	200	200	1.5	10	4	2.3707×10^{-3}
41	200	200	1.5	10	4	1.0601×10^{-3}
21	200	200	1.5	10	4	2.8097×10^{-3}
121	200	200	1.5	10	6	5.6592×10^{-3}
101	200	200	1.5	10	6	3.5610×10^{-3}
41	200	200	1.5	10	6	9.3362×10^{-4}
21	200	200	1.5	10	6	2.3665×10^{-3}

The pattern is kept for the case when $b = 1.5$, according to the results presented in the Table XXIV. Nevertheless, for $b = 2$ we do not detect the pattern anymore, as shown in the Table XXV.

6) Second Example of Geometrical Conductivity: This example is a variation of the previous one, since the red disk with radius $r = 0.2$ locates its center at $x = 0.25$ and $y = 0$. Once more, the red disk represents $\sigma = 100$, and the rest of the domain possesses $\sigma = 10$. The boundary condition is again the expression (40).

This example is interesting, because it possesses a pattern between the number of base functions M and the values of the errors $\mathcal{E}$ when $b = 1$ and $b = 1.5$, according to the values shown in the Tables XXVI and XXVII. The exception appears when $b = 2$, as reported in the Table XXVIII.

7) Third Example of Geometrical Conductivity: For this case, the conductivity function is composed as follows: one disk with radius $r_1 = 0.2$ representing $\sigma = 100$, the ring delimited by $r_2 = 0.4$ and r_1 possessing a conductivity $\sigma = 30$, another ring between $r_3 = 0.6$ and r_2 having $\sigma = 20$, whereas the one within $r_4 = 0.8$ and r_3 exhibits $\sigma = 15$. Finally, the remaining value within the boundary is $\sigma = 10$. One more time, the boundary condition is the expression (40). The behavior of the method is only stable for the case when $b = 1$. The cases $b = 1.5$ and $b = 2$ do not show any patterns to be discussed. The results are summarized in the Table XXIX.

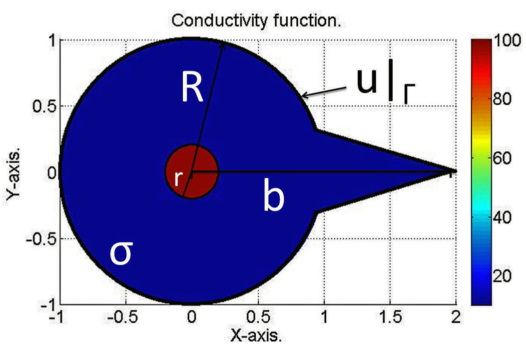

Fig. 6. First example of geometrical conductivity within a non-smooth domain. The red disk represents $\sigma = 100$ and the blue section $\sigma = 10$.

TABLE XIX
POLYNOMIAL CONDUCTIVITY IN NON-SMOOTH DOMAIN: THIRD EXAMPLE.

M	P	Q	b	α	C	$\mathcal{E}$
121	200	200	2.0	10	2	5.9419×10^{-2}
101	200	200	2.0	10	2	4.4223×10^{-2}
41	200	200	2.0	10	2	3.9702×10^{-3}
21	200	200	2.0	10	2	9.2331×10^{-3}
121	200	200	2.0	10	4	7.5193×10^{-2}
101	200	200	2.0	10	4	5.5540×10^{-2}
41	200	200	2.0	10	4	3.4802×10^{-3}
21	200	200	2.0	10	4	8.2482×10^{-3}
121	200	200	2.0	10	6	1.2689×10^{-2}
101	200	200	2.0	10	6	1.2223×10^{-2}
41	200	200	2.0	10	6	3.0911×10^{-3}
21	200	200	2.0	10	6	7.5234×10^{-3}

TABLE XX
SINUSOIDAL CONDUCTIVITY FUNCTION.

M	P	Q	b	α	ω	$\mathcal{E}$
121	200	200	1.0	10	2	1.5628×10^{-4}
101	200	200	1.0	10	2	2.2878×10^{-4}
41	200	200	1.0	10	2	1.1579×10^{-3}
21	200	200	1.0	10	2	4.9768×10^{-3}
121	200	200	1.0	10	4	1.5644×10^{-4}
101	200	200	1.0	10	4	2.3374×10^{-4}
41	200	200	1.0	10	4	2.6001×10^{-3}
21	200	200	1.0	10	4	4.3351×10^{-3}
121	200	200	1.0	10	6	1.7351×10^{-4}
101	200	200	1.0	10	6	2.6993×10^{-4}
41	200	200	1.0	10	6	1.2813×10^{-2}
21	200	200	1.0	10	6	7.1034×10^{-2}
121	200	200	1.0	10	8	7.1695×10^{-4}
101	200	200	1.0	10	8	1.0520×10^{-3}
41	200	200	1.0	10	8	5.2719×10^{-2}
21	200	200	1.0	10	8	7.7114×10^{-2}
121	200	200	1.0	10	10	7.9694×10^{-4}
101	200	200	1.0	10	10	1.1403×10^{-3}
41	200	200	1.0	10	10	6.7853×10^{-2}
21	200	200	1.0	10	10	8.2767×10^{-2}

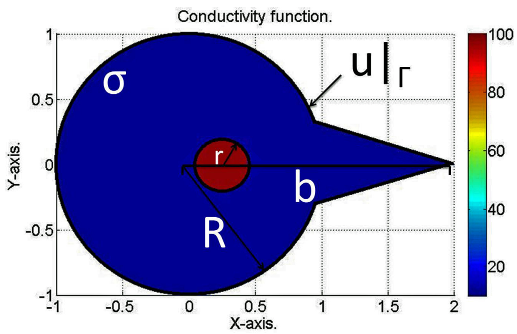

Fig. 7. Second example of geometrical conductivity within a non-smooth domain. The red disk represents $\sigma = 100$ and the blue section $\sigma = 10$.

TABLE XXI
SINUSOIDAL CONDUCTIVITY FUNCTION: A SECOND EXAMPLE.

M	P	Q	b	α	ω	$\mathcal{E}$
121	200	200	1.5	10	2	2.3734×10^{-3}
101	200	200	1.5	10	2	1.7035×10^{-3}
41	200	200	1.5	10	2	1.2907×10^{-3}
21	200	200	1.5	10	2	5.3456×10^{-3}
121	200	200	1.5	10	4	3.5305×10^{-3}
101	200	200	1.5	10	4	2.2305×10^{-3}
41	200	200	1.5	10	4	1.4848×10^{-3}
21	200	200	1.5	10	4	4.6142×10^{-2}
121	200	200	1.5	10	6	1.9220×10^{-2}
101	200	200	1.5	10	6	1.1637×10^{-2}
41	200	200	1.5	10	6	1.8806×10^{-2}
21	200	200	1.5	10	6	9.3615×10^{-2}
121	200	200	1.5	10	8	1.2419×10^{-1}
101	200	200	1.5	10	8	8.3360×10^{-2}
41	200	200	1.5	10	8	6.3304×10^{-2}
21	200	200	1.5	10	8	9.2504×10^{-2}
121	200	200	1.5	10	10	1.0707×10^{-1}
101	200	200	1.5	10	10	6.8588×10^{-1}
41	200	200	1.5	10	10	8.5009×10^{-2}
21	200	200	1.5	10	10	1.0212×10^{-1}

TABLE XXII
SINUSOIDAL CONDUCTIVITY FUNCTION: A THIRD EXAMPLE.

M	P	Q	b	α	ω	$\mathcal{E}$
121	200	200	2.0	10	2	7.8761×10^{-2}
101	200	200	2.0	10	2	5.9083×10^{-2}
41	200	200	2.0	10	2	4.7198×10^{-3}
21	200	200	2.0	10	2	3.4681×10^{-2}
121	200	200	2.0	10	4	3.3441×10^{-1}
101	200	200	2.0	10	4	2.4975×10^{-1}
41	200	200	2.0	10	4	1.4579×10^{-2}
21	200	200	2.0	10	4	8.3672×10^{-2}
121	200	200	2.0	10	6	5.7939×10^{-1}
101	200	200	2.0	10	6	4.1222×10^{-1}
41	200	200	2.0	10	6	6.3855×10^{-2}
21	200	200	2.0	10	6	1.0279×10^{-1}
121	200	200	2.0	10	8	5.7939×10^{-1}
101	200	200	2.0	10	8	4.1222×10^{-1}
41	200	200	2.0	10	8	6.3835×10^{-2}
21	200	200	2.0	10	8	1.0279×10^{-1}
121	200	200	2.0	10	10	6.5661×10^{-1}
101	200	200	2.0	10	10	4.9436×10^{-1}
41	200	200	2.0	10	10	9.5676×10^{-2}
21	200	200	2.0	10	10	1.1995×10^{-1}

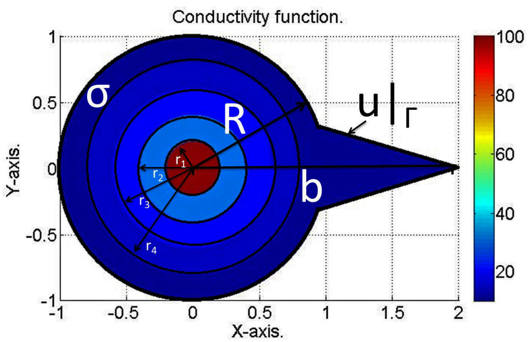

Fig. 8. Third example of geometrical conductivity within a non-smooth domain. Combination of a disk and concentric rings, within a non-smooth domain.

8) Fourth Example of Geometrical Conductivity: To describe the conductivity posed in Figure 9 is better to resemble the square within the unit circle posed before. For this case, the unit circle shall be substituted for the non-smooth domain described at the beginning of the Section. We shall only

TABLE XXIII
FIRST CASE OF GEOMETRICAL CONDUCTIVITY: $b = 1$.

M	P	Q	b	r	$\mathcal{E}$
121	200	200	1.0	0.2	5.2372×10^{-4}
101	200	200	1.0	0.2	6.6056×10^{-4}
41	200	200	1.0	0.2	1.2839×10^{-3}
21	200	200	1.0	0.2	4.5100×10^{-3}
121	200	200	1.0	0.4	5.0633×10^{-4}
101	200	200	1.0	0.4	5.9736×10^{-4}
41	200	200	1.0	0.4	1.1950×10^{-3}
21	200	200	1.0	0.4	4.5522×10^{-3}
121	200	200	1.0	0.6	2.7401×10^{-4}
101	200	200	1.0	0.6	3.2291×10^{-4}
41	200	200	1.0	0.6	1.1389×10^{-3}
21	200	200	1.0	0.6	4.8769×10^{-3}
121	200	200	1.0	0.8	4.3356×10^{-4}
101	200	200	1.0	0.8	4.6767×10^{-4}
41	200	200	1.0	0.8	1.4232×10^{-3}
21	200	200	1.0	0.8	5.3167×10^{-3}

TABLE XXIV
FIRST CASE OF GEOMETRICAL CONDUCTIVITY: $b = 1.5$.

M	P	Q	b	r	$\mathcal{E}$
121	200	200	1.5	0.2	9.5416×10^{-3}
101	200	200	1.5	0.2	6.2105×10^{-3}
41	200	200	1.5	0.2	1.9162×10^{-3}
21	200	200	1.5	0.2	4.4915×10^{-3}
121	200	200	1.5	0.4	1.0555×10^{-2}
101	200	200	1.5	0.4	6.5522×10^{-3}
41	200	200	1.5	0.4	1.7201×10^{-3}
21	200	200	1.5	0.4	4.3942×10^{-3}
121	200	200	1.5	0.6	1.0426×10^{-2}
101	200	200	1.5	0.6	6.5709×10^{-3}
41	200	200	1.5	0.6	1.7658×10^{-3}
21	200	200	1.5	0.6	4.2230×10^{-3}
121	200	200	1.5	0.8	5.8011×10^{-3}
101	200	200	1.5	0.8	3.8069×10^{-3}
41	200	200	1.5	0.8	1.7020×10^{-3}
21	200	200	1.5	0.8	3.9797×10^{-3}

remembered that the apothem $a = 0.65$, and all corners of the square are equidistant to the center of the semicircle section. The square possesses a conductivity $\sigma = 100$, whereas the remaining domain possesses $\sigma = 10$. The boundary condition is again the expression (40).

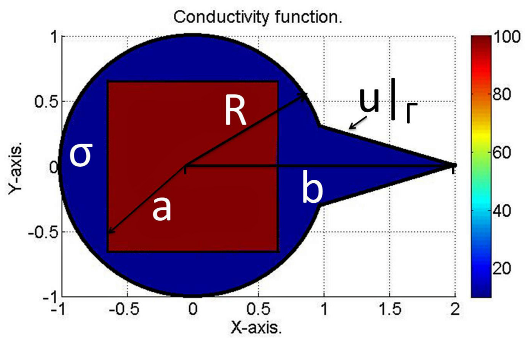

Fig. 9. Fourth example of geometrical conductivity within a non-smooth domain.

The relevance of this case is given by the multiple non-smoothness included in the geometrical conductivity. This is three non-smooth points are located at the boundary Γ, and four non-smooth points are presented in the figure within the domain Ω. For every point of non-smoothness, one radius was forced to pass on, hence all points were taken into consideration. We shall remark, as it was done in [11], that

TABLE XXV
FIRST CASE OF GEOMETRICAL CONDUCTIVITY: $b = 2$.

M	P	Q	b	r	$\mathcal{E}$
121	200	200	2.0	0.2	1.1542×10^{-1}
101	200	200	2.0	0.2	8.6105×10^{-2}
41	200	200	2.0	0.2	5.5541×10^{-3}
21	200	200	2.0	0.2	1.2137×10^{-2}
121	200	200	2.0	0.4	8.8265×10^{-2}
101	200	200	2.0	0.4	6.6393×10^{-2}
41	200	200	2.0	0.4	5.5459×10^{-3}
21	200	200	2.0	0.4	1.2121×10^{-2}
121	200	200	2.0	0.6	6.6141×10^{-2}
101	200	200	2.0	0.6	4.8414×10^{-2}
41	200	200	2.0	0.6	5.0902×10^{-3}
21	200	200	2.0	0.6	1.1946×10^{-2}
121	200	200	2.0	0.8	7.9164×10^{-2}
101	200	200	2.0	0.8	5.8350×10^{-2}
41	200	200	2.0	0.8	4.8985×10^{-3}
21	200	200	2.0	0.8	1.1917×10^{-2}

TABLE XXVI
FIRST CASE OF GEOMETRICAL CONDUCTIVITY: $b = 1$.

M	P	Q	b	r	$\mathcal{E}$
121	200	200	1.0	0.2	2.4385×10^{-2}
101	200	200	1.0	0.2	2.8740×10^{-2}
41	200	200	1.0	0.2	5.4220×10^{-2}
21	200	200	1.0	0.2	9.2323×10^{-2}
121	200	200	1.0	0.4	2.8627×10^{-3}
101	200	200	1.0	0.4	3.2700×10^{-3}
41	200	200	1.0	0.4	4.7071×10^{-3}
21	200	200	1.0	0.4	5.9983×10^{-3}
121	200	200	1.0	0.6	1.9667×10^{-3}
101	200	200	1.0	0.6	2.1911×10^{-3}
41	200	200	1.0	0.6	2.8597×10^{-3}
21	200	200	1.0	0.6	5.0975×10^{-3}

TABLE XXVII
FIRST CASE OF GEOMETRICAL CONDUCTIVITY: $b = 1.5$.

M	P	Q	b	r	$\mathcal{E}$
121	200	200	1.5	0.2	8.2351×10^{-2}
101	200	200	1.5	0.2	5.4311×10^{-2}
41	200	200	1.5	0.2	5.4607×10^{-2}
21	200	200	1.5	0.2	9.2429×10^{-2}
121	200	200	1.5	0.4	1.4896×10^{-3}
101	200	200	1.5	0.4	9.5441×10^{-3}
41	200	200	1.5	0.4	4.9048×10^{-3}
21	200	200	1.5	0.4	6.1276×10^{-3}
121	200	200	1.5	0.6	1.0957×10^{-2}
101	200	200	1.5	0.6	1.0532×10^{-2}
41	200	200	1.5	0.6	3.3790×10^{-3}
21	200	200	1.5	0.6	4.7420×10^{-3}

TABLE XXVIII
FIRST CASE OF GEOMETRICAL CONDUCTIVITY: $b = 2$.

M	P	Q	b	r	$\mathcal{E}$
121	200	200	2.0	0.2	1.9481×10^{-1}
101	200	200	2.0	0.2	1.4364×10^{-1}
41	200	200	2.0	0.2	5.7088×10^{-2}
21	200	200	2.0	0.2	9.3510×10^{-2}
121	200	200	2.0	0.4	9.5951×10^{-2}
101	200	200	2.0	0.4	7.2123×10^{-2}
41	200	200	2.0	0.4	6.6501×10^{-3}
21	200	200	2.0	0.4	1.1058×10^{-2}
121	200	200	2.0	0.6	9.0504×10^{-3}
101	200	200	2.0	0.6	7.6307×10^{-3}
41	200	200	2.0	0.6	5.5504×10^{-3}
21	200	200	2.0	0.6	1.0790×10^{-2}

not any additional regularization method was employed to warrant the convergence at the non-smooth points. This is a particular characteristic of the method, first noticed in [9], and shall be studied with more detail in further works.

TABLE XXIX
THIRD EXAMPLE OF GEOMETRICAL CONDUCTIVITY WITHIN A NON-SMOOTH DOMAIN: $b = 1,\ 1.5,\ 2$.

M	P	Q	b	$\mathcal{E}$
121	200	200	1.0	2.3863×10^{-4}
101	200	200	1.0	3.4388×10^{-4}
41	200	200	1.0	1.4742×10^{-3}
21	200	200	1.0	5.0487×10^{-3}
121	200	200	1.5	5.7241×10^{-3}
101	200	200	1.5	3.2691×10^{-3}
41	200	200	1.5	2.2058×10^{-3}
21	200	200	1.5	7.8255×10^{-3}
121	200	200	2.0	1.1136×10^{-1}
101	200	200	2.0	8.2529×10^{-2}
41	200	200	2.0	8.4147×10^{-3}
21	200	200	2.0	1.4548×10^{-2}

The Table XXX presents a summary of the calculations performed for this last example. Only for the case when $b = 1$ a pattern between the number of base elements M and the error $\mathcal{E}$ is observed. The other two cases do not report any visible pattern.

TABLE XXX
FOURTH EXAMPLE OF GEOMETRICAL CONDUCTIVITY IN NON-SMOOTH DOMAIN.

M	P	Q	b	$\mathcal{E}$
121	200	200	1.0	8.1631×10^{-3}
101	200	200	1.0	1.0347×10^{-2}
41	200	200	1.0	3.3239×10^{-2}
21	200	200	1.0	7.3480×10^{-2}
121	200	200	1.5	1.1063×10^{-1}
101	200	200	1.5	7.5019×10^{-2}
41	200	200	1.5	4.3609×10^{-2}
21	200	200	1.5	9.1848×10^{-2}
121	200	200	2.0	4.3692×10^{-1}
101	200	200	2.0	3.2518×10^{-1}
41	200	200	2.0	6.1231×10^{-2}
21	200	200	2.0	1.2170×10^{-1}

ACKNOWLEDGEMENT

The authors would like to acknowledge the support of CONACyT projects 106722 and 81599; A. G. Bucio R. thanks to UPIITA-IPN and CONACyT; M.P. Ramirez T. acknowledges the support of HILMA S.A. de C.V.; C. M. A. Robles G. would like to thank La Salle University for the research stay and to CONACyT.

REFERENCES

[1] K. Astala, L. Päivärinta (2006), *Calderon's inverse conductivity problem in the plane*, Annals of Mathematics, Vol. 163, pp. 265-299.

[2] L. Bers (1953), *Theory of Pseudoanalytic Functions*, IMM, New York University.

[3] A. Bucio R., R. Castillo-Perez, M.P. Ramirez T.,C.M.A. Robles G. (2012), *A Simplified Method for Numerically Solving the Impedance Equation in the Plane*, 9th International Conference on Electrical Engineering, Computing Science and Automatic Control 2012, IEEE Catalog Number: CFP12827-CDR, ISBN: 978-1-4673-2168-6.

[4] A. P. Calderon (1980), *On an inverse boundary value problem*, Seminar on Numerical Analysis and its application to Continuum Physics.

[5] H. M. Campos, R. Castillo-Perez, V. V. Kravchenko (2011), *Construction and application of Bergman-type reproducing kernels for boundary and eigenvalue problems in the plane*, Complex Variables and Elliptic Equations, 1-38.

[6] R. Castillo-Perez., V. Kravchenko, R. Resendiz V. (2011), *Solution of boundary value and eigenvalue problems for second order elliptic operators in the plane using pseudoanalytic formal powers*, Mathematical Methods in the Applied Sciences, Vol. 34, Issue 4.

[7] V. V. Kravchenko (2009), *Applied Pseudoanalytic Function Theory*, Series: Frontiers in Mathematics, ISBN: 978-3-0346-0003-3.

[8] V. V. Kravchenko (2005), *On the relation of pseudoanalytic function theory to the two-dimensional stationary Schrödinger equation and Taylor series in formal powers for its solutions*, Journal of Physics A: Mathematical and General, Vol. 38, No. 18, pp. 3947-3964.

[9] M. P. Ramirez T., R. A. Hernandez-Becerril, M. C. Robles G. (2012), *Study of the Numerical Solutions for the Electrical Impedance Equation in the Plane: A Pseudoanalytic approach of the Forward Dirichlet Boundary Value Problem*, Mathematical Methods in the Applied Sciences (submited for publication). Available in electronic format at http://ArXiv.com

[10] C. M. A. Robles G., A. Bucio R., M. P. Ramirez T. (2012), *An Optimized Numerical Method for Solving the Two-Dimensional Impedance Equation*, Lecture Notes in Engineering and Computer Science: Proceedings of The World Congress on Engineering and Computer Science 2012, WCECS 2012, 24-26 October, 2012, San Francisco, USA, pp. 116-121.

[11] C. M. A. Robles G., A. Bucio R., M. P. Ramirez T., V. D. Sanchez N. (to be published), *On the Numerical Solutions of Boundary Value Problems in the plane for the Electrical Impedance Equation: A Pseudoanalytic Approach for Non-Smooth Domains*, Lecture Notes in Electrical Engineering, IAENG Transactions on Engineering Technologies-Special Issue of the World Congress On Engineering and Computer Science 2012, Springer.

[12] I. N. Vekua (1962), *Generalized Analytic Functions,* International Series of Monographs on Pure and Applied Mathematics, Pergamon Press.

[13] J. G. Webster (1990), *Electrical Impedance Tomography*, Adam Hilger Series on Biomedical Engineering.